INVESTIGATIONS OF AMINO ACID-BASED SURFACTANTS AT LIQUID INTERFACES

A Thesis

by

DENGLIANG YANG

Submitted to the Office of Graduate Studies of
Texas A&M University
in partial fulfillment of the requirements for the degree of

MASTER OF SCIENCE

August 2004

Major Subject: Chemistry

INVESTIGATIONS OF AMINO ACID-BASED SURFACTANTS AT LIQUID INTERFACES

A Thesis

by

DENGLIANG YANG

Submitted to Texas A&M University
in partial fulfillment of the requirements
for the degree of

MASTER OF SCIENCE

Approved as to style and content by:

Paul S. Cremer (Chair of Committee)	François P. Gabbaï (Member)
David P. Giedroc Member)	Emile A. Schweikert (Head of Department)

August 2004

Major Subject: Chemistry

ABSTRACT

Investigations of Amino Acid-Based Surfactants at Liquid Interfaces.

(August 2004)

Dengliang Yang, B.E., Zhejiang University;

M.S., National University of Singapore

Chair of Advisory Committee: Dr. Paul S. Cremer

Herein are presented collective studies of amino acid-based surfactants, also known as lipoamino acids, at liquid interfaces. Chapter III describes an investigation of domain morphology of *N*-Stearoylglutamic acid (*N*-SGA) Langmuir monolayers at the air/water interface by epifluorescence microscopy. Anisotropic feather-like domains were observed in $_{L}$-enantiomeric monolayers while symmetric circular domains were found in racemic *N*-SGA monolayers. At a surface pressure of 30 mN/m the enantiomeric domains melted at 31 °C while the racemic domains melted at 27 °C. This result is exactly opposite to the behavior found in bulk crystals where the racemate melts at a higher temperature. These results were explained in terms of different molecular packing and hydrogen bonding between bulk crystals and two-dimensional thin films for enantiomeric and racemic compounds. Chapter IV summarizes the investigations of hydrogen bonding in *N*-acyl amino acid monolayers by vibrational sum-frequency spectroscopy (VSFS). The intermolecular hydrogen bonding interaction between the

adjacent molecules through amide-amide groups in *N*-stearoylalanine (*N*-SA) is characterized by an NH stretch peak at 3311 cm^{-1}. This is the first time that the amide NH stretching signals have been detected with the VSFS technique. A similar peak was detected at 3341 cm^{-1} on *N*-SGA monolayer. The higher frequency indicates that the H-bond strength is weaker due to the larger size of the glutamic acid residue. The NH stretch mode can thus be used as a fingerprint of hydrogen bonding among amide-amide groups. A peak at 3050 cm^{-1} due to hydrogen bonding among carboxyl groups was also resolved from the VSFS spectra. Molecular models of intermolecular hydrogen bonding were proposed.

ACKNOWLEDGMENTS

This thesis concludes my graduate study in the Chemistry Department of Texas A&M University from Spring 2003 to Summer 2004. I owe great thanks to many people for the completion this work.

First of all, I want to thank my advisor, Dr. Paul Cremer, for his guidance in research. Paul gave me a tremendous amount of freedom to explore unknown areas in surface chemistry. He was always able to provoke new thoughts on my research from a very fundamental point of view. This will remain an inspirational source for my future research work.

Next, there is a group of people I wish to thank for their friendship and help with my scientific work. Tinglu is a great source of encouragement and wisdom for both research and life. Without his help with microscopy, it would not have been possible to start the project of investigating monolayer domains. Hanbin is a former student from the Cremer group, from whom I learned about research in chemistry, although the time interacting with him was short. It was also very pleasant to share scientific discussions with Yanjie, Tao and recently JianJun on a daily basis. The rest of the Cremer group is also acknowledged for their support.

I would also like to thank my committee members for their valuable time and guidance. Dr. Giedroc has been very supportive from beginning. Dr. Gabbaï is very kind to serve on my committee on such short notice. He provided valuable suggestions on crystal growth as well.

Finally, I owe a huge debt to my parents, Zuochen Yang and Manao Bao, for their continuing encouragement of my studies over the years. I have been away from home for my education for ten years now. Without their support, I could not have gone so far. I also wish to thank Chunmei for a tremendous amount of help in my writing and other matters.

TABLE OF CONTENTS

LIST OF FIGURES

FIGURE Page

CHAPTER I

INTRODUCTION

Amino acid-based surfactants (AAS), also known as lipoamino acids, are one category of biological-based surfactants. They have a number of attractive properties such as chemical simplicity, surface activity, biological activity and biocompatibility. The lipoamino acids occur naturally in microorganism cell walls. Since 1963 a series of lipoamino acid molecules have been discovered in microorganisms.[1] The biosynthesis of *N*-acyl amino acid in the marine bacterium, *Deleya marina*, was reported in 1997.[2] In 2004, a new bacterial *N*-acyl $_{D}$-amino acid was isolated from *Bacillus pumilus* IM 1801.[3] Although the *in vivo* physiological functions of these compounds are still unknown, a few applications have been proposed and demonstrated in pharmaceutical, cosmetic and household applications.[4] A new class of *N*-acyl glycine molecules was also found in bovine and rat brains that suppresses inflammatory pain.[5] Because of the chemical simplicity of amino acid-based surfactants, they can be readily synthesized in the laboratory. Also, all the amino acids except glycine, possess a chiral center, therefore these surfactants have chirality, which is prevalent in biological systems. Due to the amphiphilic nature and bio-relevance of these molecules, their surface activities are deemed interesting for fundamental investigations, especially in the area of biological surface chemistry.

Despite the potential interest of AAS in fundamental research, literature reports of the properties of this category of molecules are scant. Information about preparation,

---

This thesis follows the format and style of *Langmuir*.

structure and properties of AAS is found mostly in the Japanese patent literature. The general structure of *N*-acyl amino acids is shown in Figure 1. The amino acids are connected to long-chain fatty acids through an amide bond. Typically, their hydrocarbon chains have 14-18 carbons as previously reported.[4] The molecules are amphiphilic as they have a polar amino acid on one end and a long hydrocarbon chain as a nonpolar group on the other end. There is also a chiral carbon center that the amino acid residues (except glycine) are connected to. This property makes AAS molecules ideal objects to study chiral molecular interactions.

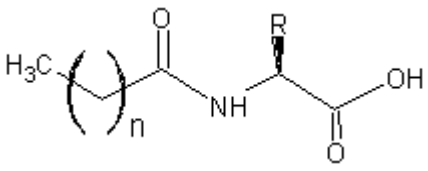

Amino acids	Residues (-R)
Gly	-H
Ala	$-CH_3$
Glu	$-CH_2CH_2COOH$

Figure 1. Chemical structure of *N*-acyl amino acids.

Surfactants (short for surface-active agents) consist of a hydrophilic (water-like) head group and a hydrophobic (water-repellent) hydrocarbon tail. They have some interesting interfacial properties that are of great theoretical and practical significance. When the hydrophobic tail is long enough, the molecules will orient themselves at the air/water interface to minimize their free energy. The surface film is one molecular layer thick and is usually called a monomolecular layer or monolayer. In 1917, Irving

Langmuir put forward evidence for the monomolecular nature of the film and the orientation of the molecules at interface.[6] The monomolecular film is also called a Langmuir film or a Langmuir monolayer for historical reasons. In the Langmuir monolayer, the polar end is directed towards the water and the hydrocarbon tail toward the air as illustrated in Figure 2a. The amphiphilic molecules can also associate into a variety of structures in an aqueous solution. Above a critical micelle concentration (CMC), the molecules can also spontaneously aggregate into micelles as shown in Figure 2b. The driving force is derived from the hydrophobic attraction at the hydrocarbon-water interface, which induces the molecules to associate. The hydrophilic, ionic or steric repulsion of the head groups imposes the requirement for them to contact with water.

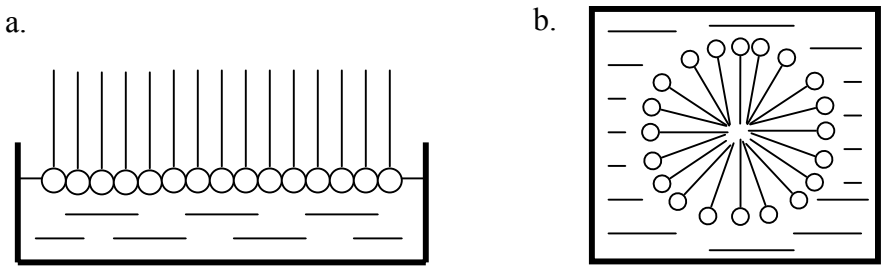

Figure 2. Schematic representation of surfactant assembly. (a) a Langmuir monolayer at air/water interface; (b) a micelle in aqueous solution.

When the monolayer is compressed at the air/water interface, it will undergo several phase transformations, which are analogous to three-dimensional phases such as gases, liquids and solids. The state of the monolayer may be monitored by the surface

pressure as a function of the area occupied by the molecules. Figure 3 shows a plot of the two-dimensional equivalent of the pressure versus volume isotherm for bulk states. The two dimensions in the plane of the surface lead to a total kinetic energy of kT, which is assumed to produce the surface pressure, and thus lead to an ideal two-dimensional gas equation[7]

$$\Pi A = kT \tag{1.1}$$

where Π is surface pressure in mN/m, A is the molecular area in $Å^2$/molecule and kT is the total kinetic energy. In the 'gaseous' state (G in Figure 3), the molecules are far enough apart that they have little effect on each other. As the surface area of the monolayer is reduced, the hydrocarbon chains start to interact. The 'liquid' state is also called an expanded monolayer phase (E). With the molecular area progressively reduced, condensed (C) phases may appear. In this state, the molecules are closely packed and are oriented with the hydrocarbon chain pointing away from the water surface.[8]

The coexistence of the condensed and the expanded phases may be observed directly by doping the monolayer with a small amount of fluorescence dye. The dye generally has different solubility or fluorescence quantum yield in the coexisting phases, which provide ample contrast to image phase domains as shown in Figure 4.[9] Due to the chiral nature of the molecules in the monolayer, the phase domains posses some asymmetric features. The microstructures and phase transitions in lipid monolayers have been extensively studied.[10] A successful theoretic model was proposed by McConnell to account for the competition between electrostatic dipole-dipole interactions and line tensions of domains.[11]

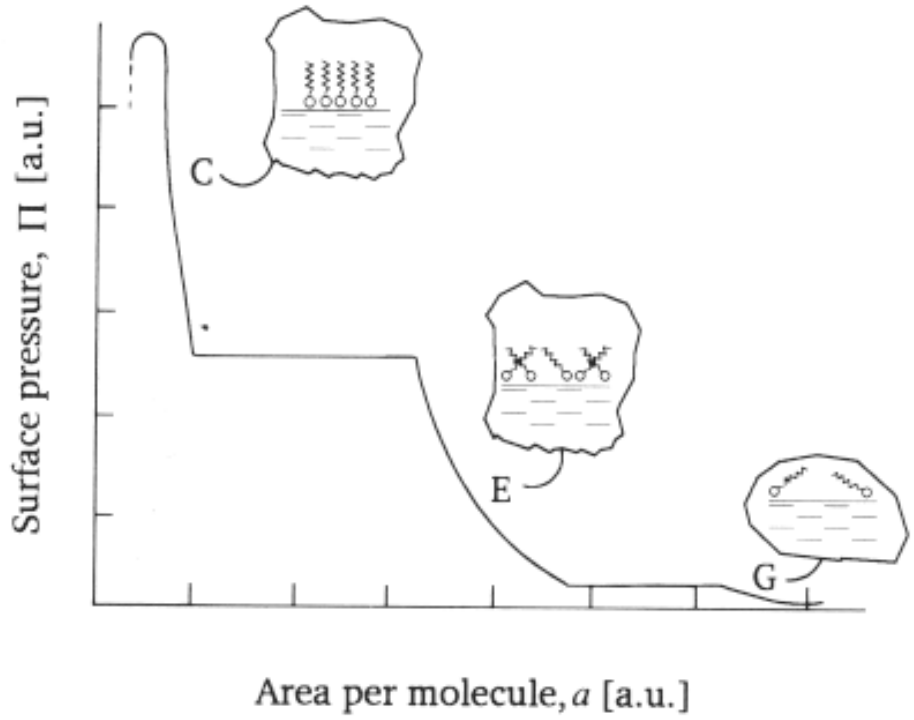

Figure 3. A schematic surface pressure area isotherm illustrating the states of a monolayer.[8] G is short for gaseous state, E is short for expanded monolayer phase and C is the condensed phase.

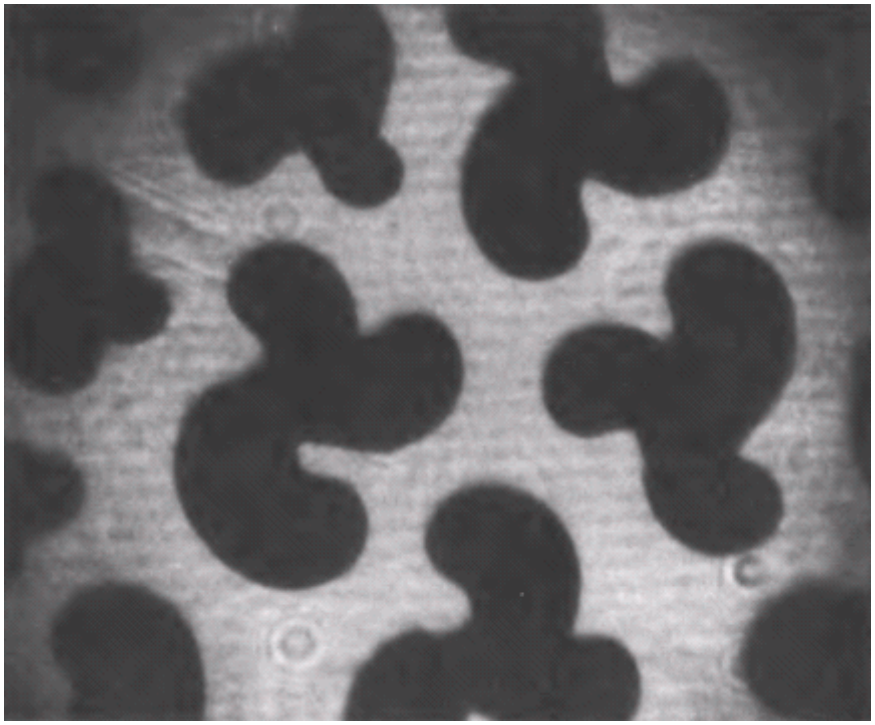

Figure 4. A fluorescence micrograph showing solid domains formed in a mixture of the two enantiomers of dipalmitoylphosphatidylcholine (DPPC). Image was taken at a pressure of 9 dyn/cm and an average molecular area of 70 $Å^2$.[9] The handedness of the condensed domains are related to the molecular chirality of DPPC.

In a first set of studies, *N*-acyl amino acids were used as a simple model system to investigate chirality effects, which are essential for the properties and functions of biomolecules such as carbohydrates, peptides and lipids. These biomimetic models can be studied more easily than their biological counterparts.[12] The chiral discrimination effect on chiral molecular interaction was found to be enhanced in two-dimensions. The molecular chirality effect is manifested by the microstructure of phase domains in the monolayers. Such micron size domains can be observed *in situ* by optical techniques

such as epifluorescence microscopy. Microscopy investigations afford a direct observation of how the handedness of molecular assemblies correlates with the phase behavior and the morphology of the Langmuir monolayers.[13] Often times, racemic crystals are more stable than enantiomeric crystals.[14] Due to the difference in molecular packing between bulk crystals and two-dimensional thin films, the molecular thermal stability may be completely reversed. Experimental investigations and molecular models of *N*-SGA are presented in Chapter III.

In a second set of studies, amino acid-based surfactants were investigated at the air/water interface by vibrational sum frequency spectroscopy (VSFS). The hydrogen bonding formation between amide groups and carboxylic groups in the *N*-acyl amino acids monolayers were studied. The results are summarized in Chapter IV.

In a final set of studies, the lipoamino acids' interactions with biomembranes are investigated. Solubilization of membranes by detergents has been intensively studied since the 1970s.[15] Amphiphilic molecules such as sodium dodecyl sulfate (SDS) were used to extract proteins from protein-containing membranes.[16] But there are very few studies of interactions of lipoamino acids with membranes. A study of lipoamino acids interacting with supported lipid bilayers will be presented at the end of the thesis.

CHAPTER II

EXPERIMENTAL

Synthesis of *N*-Acyl Amino Acids

A number of synthetic procedures have been developed over the past several years to obtain *N*-acyl amino acids.[4] The most popular method is to prepare the molecules from fatty acids and amino acid precursors involving a two-step process.[17,18,19] First, acid chlorides are prepared by reaction of the fatty acids with $SOCl_2$ solvent. Subsequently, the acid chlorides are reacted with the amino acids to yield the final products.

The preparation of *N*-stearoyl glycine (*N*-SG) is illustrated in Figure 5. 28 g of stearic acid (Aldrich, 95%) was added to 100 mL $SOCl_2$ (Aldrich, 99%) solvent in a round bottom flask while stirring. A few drops of DMF was also added. The mixture was refluxed in an oil bath for about 4 hours. The crude product is brown in color. Colorless liquid stearoyl chloride was obtained by reduced pressure distillation (2 mmHg) at 170 ^{o}C. 3.8 g of glycine (Aldrich, 99%) were dissolved in 50 mL of deionized water. The pH was adjusted to 10 by adding NaOH pellets to the solution. 20 mL of stearoyl chloride was added dropwise to the aqueous solution while stirring at 30 ^{o}C. After 1 hour, the mixture was cooled to room temperature and the pH was adjusted to 1 by adding HCl. The crude product precipitated out from the aqueous solution, which was filtered and washed with water.

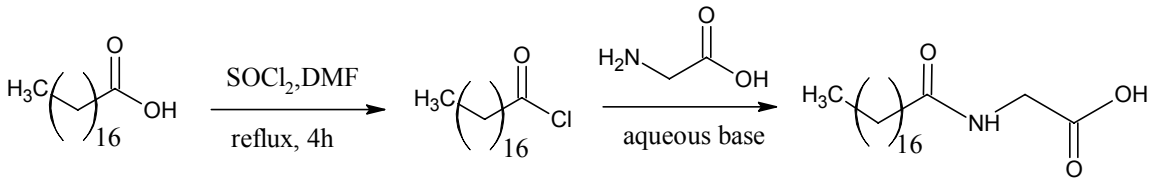

Figure 5. The synthesis of *N*-stearoyl glycine.

The white powder obtained was subsequently washed with chloroform three times and dried in a vacuum desiccator. The molecular structure was confirmed by ^{1}H NMR and FTIR. ^{1}H NMR was carried out on a VXR-300 operating at 300 MHz, with CD_3OD as the solvent and an internal standard (4.81 and 3.31 ppm). The spectrum is shown in Figure 6. The corresponding protons are labeled in the figure. An FITR spectrum was acquired in a KBr pellet as shown in Figure 7. Characteristics peaks (cm^{-1}) are found at 3339 (N-H), 1705 (C=O), 1640 (amide I) and 1542 (amide II).

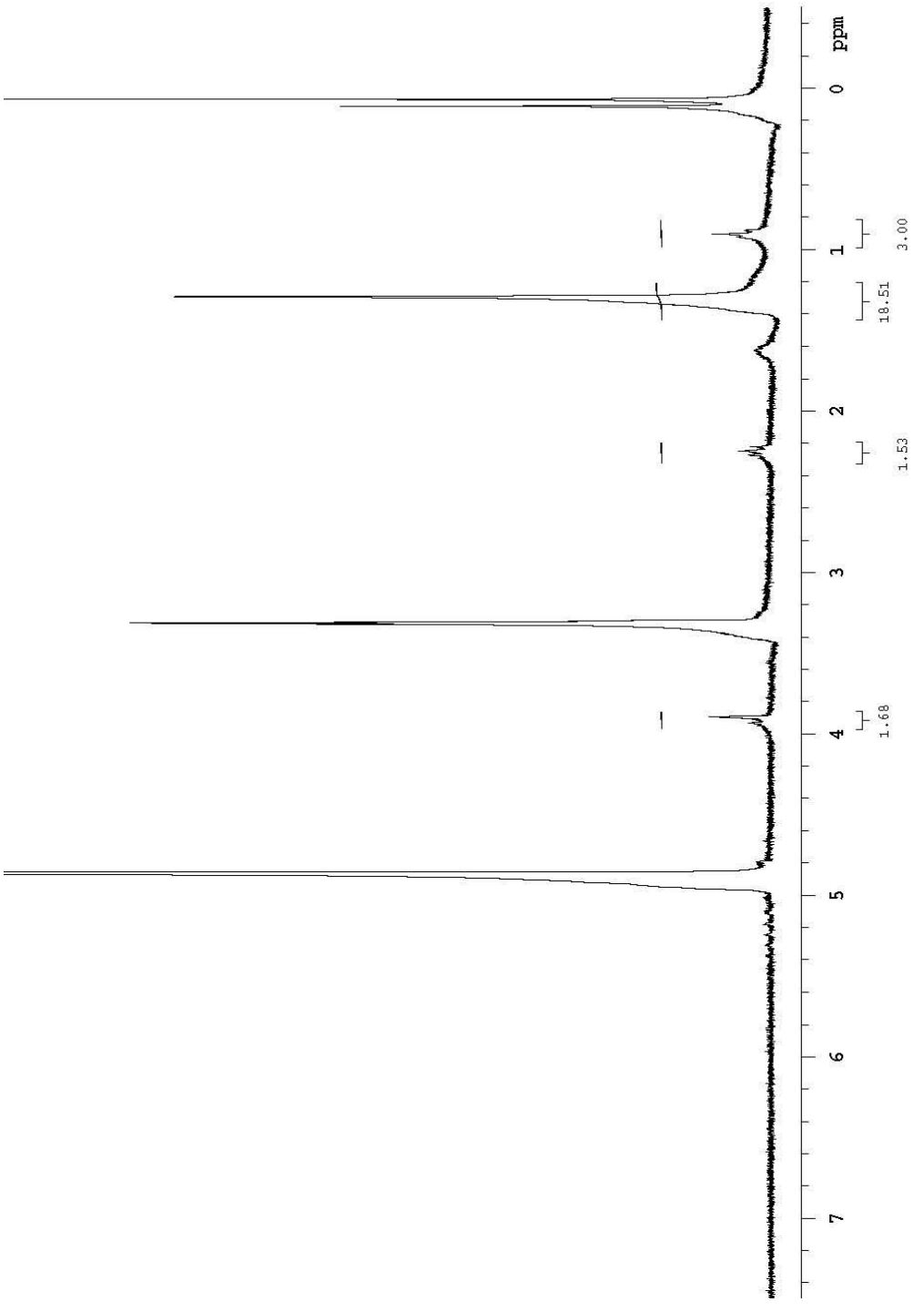

Figure 6. ^{1}H NMR spectrum of *N*-stearoyl glycine in CD_3OD solution.

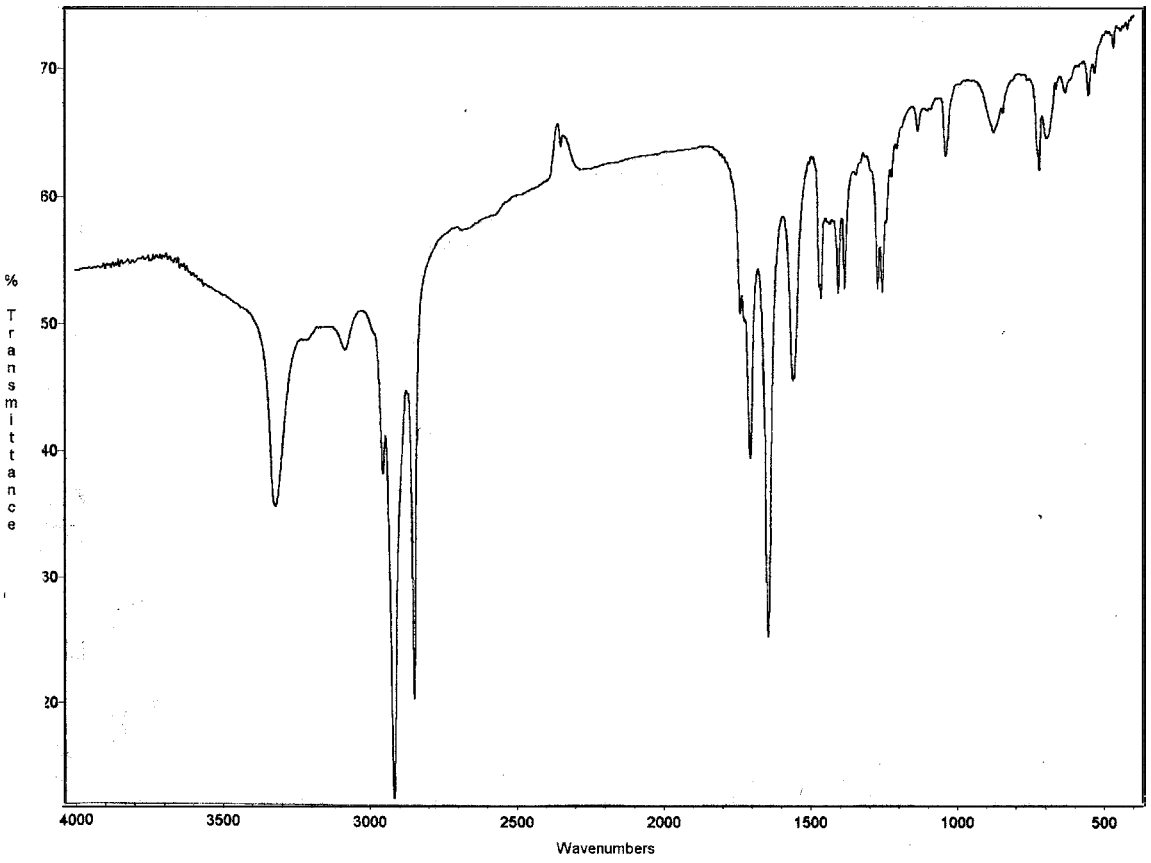

Figure 7. FTIR spectrum of *N*-stearoyl glycine in a KBr pellet.

The above reaction is quite straightforward; however, one still needs to take precautions with the reaction conditions during stearoyl chloride addition. Temperature needs to be kept at 30 ^{o}C or below. At higher temperature, hydrolysis of the stearoyl chloride into stearic acid will compete with the acylation reaction. It is also necessary to keep the pH value around 10 to have the amine group unprotonated for the acylation reaction.

The synthesis of *N*-stearoyl glutamic acid (*N*-SGA) is similar to the prepration of *N*-SG. After stearoyl chloride is prepared, enantiomeric and racemic glutamic acids can be conjugated to the precursor. The synthesis was reported earlier by Takehara[20] and Zhang.[21] Briefly, glutamic acid (1 mol) was dissolved into a water/acetone mixture. NaOH (2 mol) was added to convert the glutamic acid into disodium glutamate. Stearoyl chloride (1 mol) and NaOH (1mol) in water were added dropwise to this solution while stirring at 30 ^{o}C and pH 12. After two hours, the mixture was cooled and acidified with HCl. The precipated crude crystals were washed with petroleum ether to obtain pure crystals. At a ratio of 40 % acetone, the maximum yield of 90 % was achieved. The structures of the compounds were confirmed by FT-IR and ^{1}H NMR. ($_{L}$-enantiomer) IR (cm^{-1}): 3339 (N-H), 1731 (C=O in carboxylic acid), 1644 (amide I) and 1542 (amide II). The ^{1}H NMR measurements were carried out on a Bruker DMX-400 instrument operating at 400 MHz in CD_3SOCD_3. Characteristics chemical shift (δ, ppm) and proton information are as follows: 0.97 (t, 3H, -CH_3), 1.35 (m, 28H, -CH2-), 1.58 (t, 2H, -CH_3 attached to chiral center), 1.86 (m, 2H, -CH_2-), 2.05 (m, 2H, -CH_2-), 4.3 (m, 1H, -CH-, chiral center). The molecular structure is shown in Figure 8.

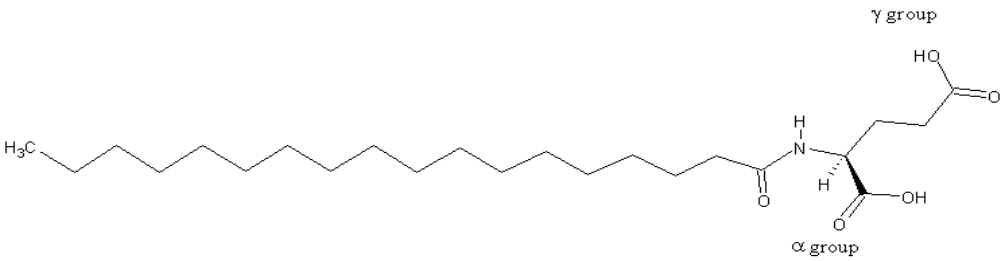

Figure 8. The molecular structure of $_{L}$-*N*-stearoylglutamic acid. The carboxylic acid groups are labeled α and γ.

Methods for Langmuir Monolayer Morphology Studies

Experiments were carried out in an apparatus called a Langmuir trough. The trough is usually made of a hydrophobic materials such as Teflon to contain the subphase water and movable barriers that span over the water surface. A schematic diagram of this apparatus is shown in Figure 9. Spreading solutions are usually prepared by dissolving molecules in volatile solvents such as chloroform. The molecules are confined on the water surface by the barriers. The molecular area in the monolayer can be changed by closing or expanding the barriers. The surface pressure is defined as the difference between the surface tension of the pure fluid and that of the film-covered surface

$$\Pi = \gamma - \gamma_0 \tag{2.1}$$

where γ and γ_0 are surface tensions in absence and presence of the monolayer. The pressure can be measured by the Wilhelmy plate method as shown Figure 10.

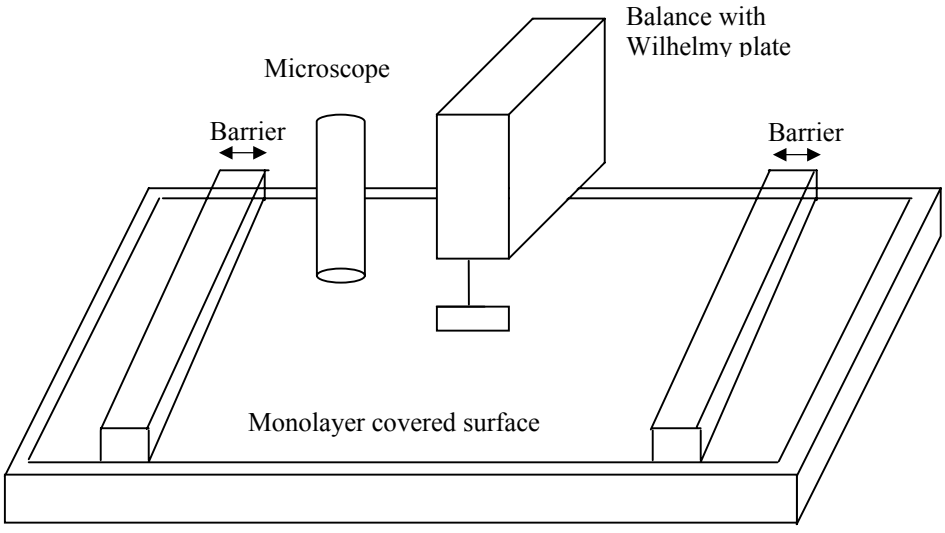

Figure 9. Schematic representation of a Langmuir trough.

In this method, a rectangular plate made of platinum or even a piece of filter paper is partially immersed in to the subphase. The force due to surface tension is measured as

$$F = \rho_p g l_p w_p t_p + 2\gamma\left(t_p w_p\right)\cos\left(\theta\right) - \rho g t_1 w_1 h_1 \tag{2.2}$$

where ρ_p is the density of the plate, ρ is the density of the liquid and θ is the contact angle of the liquid on the solid plate. If the plate is completely wet by the liquid (i.e. $\cos\left(\theta\right) = 1$), the surface pressure is determined from the following equation:

$$\Pi = -\Delta\gamma = -\left[\Delta F / 2\left(t_p + w_p\right)\right] = -\Delta F / 2w_p, if\ \ w_p \gg t_p \tag{2.3}$$

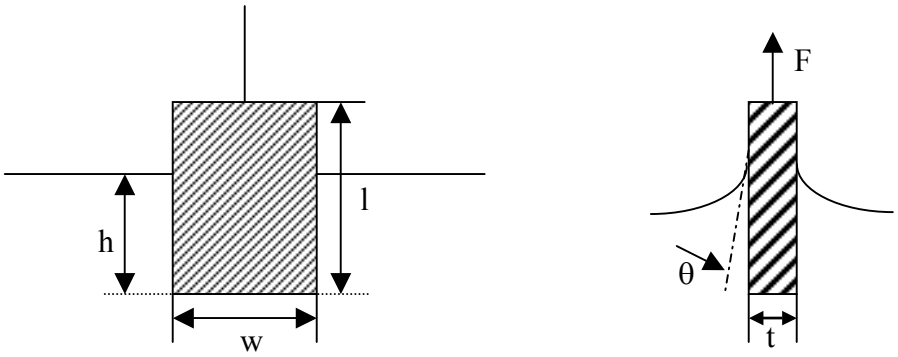

Figure 10. Wilhelmy plate method for measuring the surface pressure.

For the imaging of domain microstructure in Langmuir monolayer, a fluorescence dye is incorporated into the monolayer spreading solution. The details of the experiment in Chapter III is described in following paragraph.

The spreading solutions for monolayer formation were prepared by dissolving either the $_L$ or the racemic form of *N*-SGA into a 14:1 chloroform-ethanol solution at a

concentration of 2.3 mM. The solutions were then doped with 0.5 parts per thousand Texas Red-DHPE (Molecular Probes, Eugene, OR). NaCl and $CuCl_2$ solutions were prepared by dissolving the 99.99% pure salts into water from a NANOpure Ultrapure Water System (Barnstead, Dubuque, IA). The pH values of the solutions were adjusted by concentrated HCl and NaOH solutions. Monolayers were formed on a Nima 601M Langmuir trough (Nima Technology Ltd., England) equipped with a Wilhelmy plate for measuring the two-dimensional surface pressure. The trough could be fit onto the stage of a Nikon E800 epifluorescence microscope. The subphase temperature was controlled by a circulating water bath connected to the Teflon body of the trough. Domain observations were carried out using a 40x objective lens. All images were captured by a 1024b Micromax CCD camera and processed with Metamorph software from Universal Imaging Corp.

Vibrational Sum Frequency Spectroscopy Studies

In VSFS experiments, two input beams at frequency of ω_1 and ω_2 are focused at the interface of a medium to generate an output beam at the sum frequency of $\omega = \omega_1 + \omega_2$. Usually ω_1 is kept in the visible range while ω_2 is tuned in the infrared range to scan over the vibrational resonances of the molecules. The resonantly enhanced sum frequency response is then obtained from the sample according to the sum frequency generation selection rules as have been reviewed elsewhere[22,23]. Briefly, in the electric-dipole approximation, only media that lack inversion symmetry will have a sum frequency response. The intensity I_{SFS} is proportional to the square of second-order

nonlinear susceptibility, $\chi^{(2)}$ which can be divided into two parts, a frequency dependent resonant term, $\chi_R^{(2)}$ and a nonresonant term, $\chi_{NR}^{(2)}$.

$$I_{SFS} \propto \left|\chi^{(2)}\right|^2 I_{vis} I_{IR} = \left|\chi_R^{(2)} + \chi_{NR}^{(2)}\right| I_{vis} I_{IR} \tag{2.4}$$

where I_{vis} and I_{IR} designate the visible and IR beam intensities respectively. The resonant term can be expressed as

$$\chi_{R_n}^{(2)} = \sum_n \frac{A_n}{\omega_{IR} - \omega_n + i\Gamma_n} \tag{2.5}$$

where $A_n, \omega_n, \omega_{IR}$ and Γ_n are the oscillator strength, resonant frequency, frequency of the IR beam, and damping constant of the nth vibrational resonant mode, respectively. A_n is the product of the infrared and Raman transition dipole moments as well as a phase factor, their orientational vector average, and their number density at the interface.

The instrument in our lab has been described elsewhere[24,25]. Briefly, the 1064 nm radiation source came from a mode-locked Nd: YAG laser (PY61c, Continuum, Santa Clara, CA), operated at a 20Hz repetition rate with a peak width of 21 ps. This beam was used to pump an optical parametric generation/amplification (OPG/OPA) stage (Laser Vision, Bellevue, WA) to produce a tunable IR beam (from 2800 to 3600 cm^{-1}) in addition to a frequency doubled beam at 532 nm. A Langmuir trough (Model 601 M, Nima Technology Ltd., Coventry, England) equipped with a Wilhelmy plate was used to control the surface pressure of the amphiphilic amino acid at air/water interface. The IR and visible beams were aligned over the surface of monolayer with incident angles of 51^0 and 42^0, respectively. A schematic diagram of the instruments is shown in Figure 11.

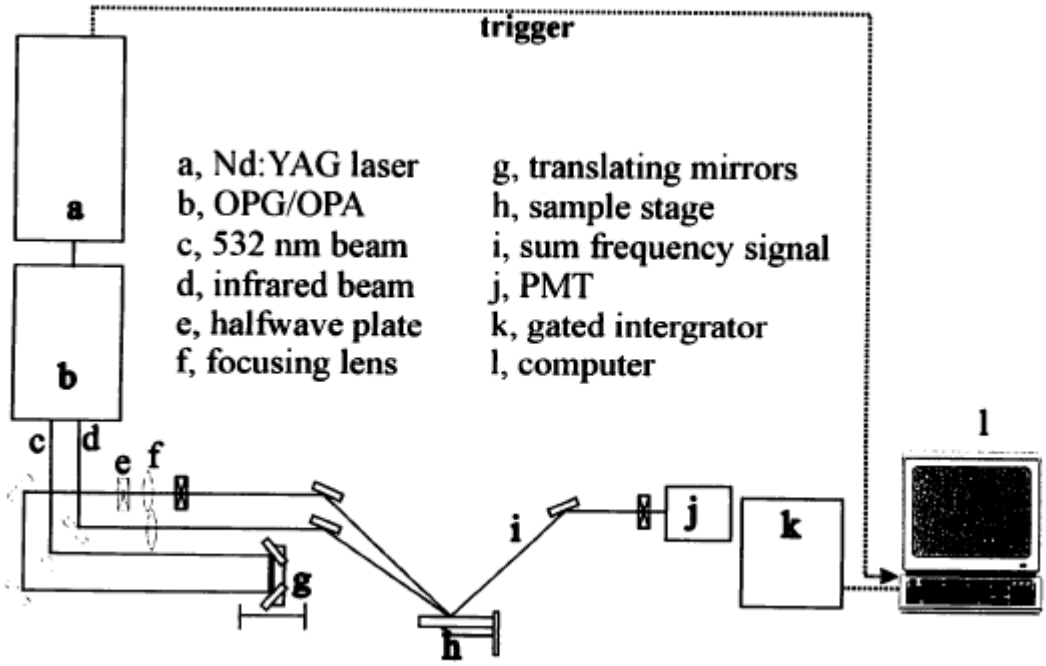

Figure 11. Schematic diagram of the VSFS system.

Methods for Supported Lipid Bilayer Studies

Solid supported lipid bilayers were prepared as previously reported. Briefly, lipids were dissolved in chloroform and allowed to dry under a stream of nitrogen followed by desiccation under vacuum for 2 h. The lipids were reconstitutioned in PBS buffer (pH 7.2) and extruded seven times through two polycarbonate filters with 50 nm pores. The lipid vesicles spontaneously fused to a well-cleaned glass surface to form a continuous planar lipid bilayer. Excess vesicles were flushed away with water. The supported bilayer used in these experiments was 99% egg phosphatidylcholine (egg PC; Avanti Polar Lipids, Alabaster, AL) and 1% Texas-Red dihexadecanoyl-phosphatidylethanolamine (TR-DHPE) (Molecular Probes, Eugene, OR).

The lateral diffusion of the lipid bilayer was determined by fluorescence recovery after photobleaching (FRAP). This method has been developed and adopted by many groups.[26,27,28] An Ar-Kr mixed gas laser was used to photobleach the fluorescence dye doped lipid bilayer. After bleaching for 2 seconds, the black spot was found as shown in Figure 12. Time lapsed pictures were taken every 5 second for 5 min. The intensity of the spots was measured afterwards with Metamorph software. The initial intensity was taken as $F_K(\infty)$, the intensity in the pot after bleaching was taken as $F_K(0)$, the fluorescence intensity recovery $\frac{F_K(t)-F_K(0)}{F_K(\infty)-F_K(0)}$ versus time is plotted in Figure 13. The data can be fit to the following equation:

$$y = y_0 + a\left(1-e^{-bx}\right) \tag{2.6}$$

The half time $t_{1/2}$ was determined from solving $f(t_{1/2}) = \frac{1}{2}$. The diffusion rate can then be determined by the following formula

$$D = \frac{w^2}{4t_{1/2}}\gamma_D \tag{2.7}$$

where w is the beam width, γ_D is determined upon beam shape, type of transport and bleaching parameter K.[26]

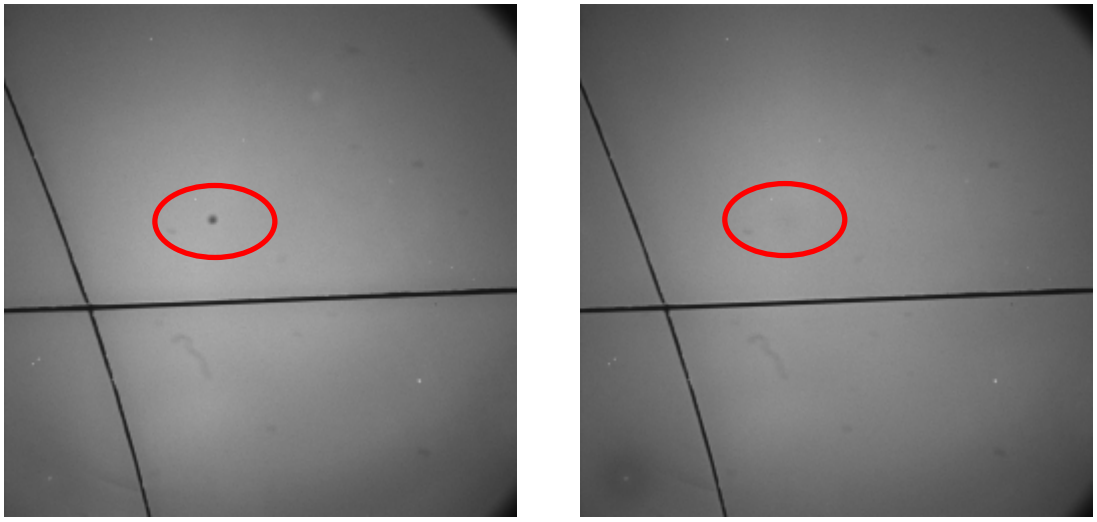

Figure 12. Images of a lipid bilayer after photobleaching and recovering.

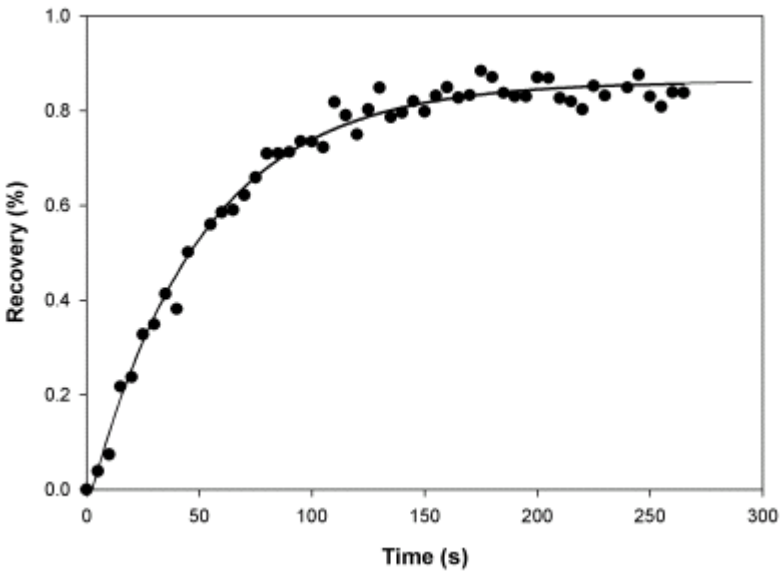

Figure 13. Fluorescence recovery curve of 1%TR-eggPC bilayer on glass.

CHAPTER III

ON THE THERMAL STABILITY AND THE DOMAIN MORPHOLOGY OF *N*-STEAROYLGLUTAMIC ACID MONOLAYERS

Introduction

Over the last two decades there has been considerable interest in the phase behavior and domain morphology of chiral molecules in Langmuir films.[12,29] Two-dimensional molecular assembly at the air/water interface can be easily manipulated to study chiral molecular recognition[30] in general and homochiral evolution[31] in specific. The molecular chirality effect is manifested by the microstructure of phase domains in the monolayers. Optical techniques such as epifluorescence microscopy and Brewster angle microscopy (BAM) allow *in situ* observations of such micron size domains.

N-acyl derivatives of amino acids have been intensively studied for their pronounced chiral discrimination effects.[13,32-35] Microscopy investigations allow a direct observation of how the handedness of molecular assemblies correlates with the phase behavior and the morphology in Langmuir monolayers.[35] Herein, we report a comparative study of the domain microstructures of *N*-SGA monolayers. The molecular structure is shown in Figure 7. The morphology of enantiomeric and racemic monolayers was studied under different subphase conditions, which revealed a striking difference in molecular interaction strengths between the enantiomeric and the racemic films. In bulk, the racemic crystals are generally more stable than the enantiomeric crystals.[14] This is also the case for the compounds we synthesized. Curiously, however, we found that the

enantiomeric monolayers were more stable than the corresponding racemates in the presence of acidified subphases at the air/water interface.

One possible explanation for the inversion of stability upon going from three dimensions to two involves the role of amide-amide hydrogen bonding (H-bonding). In fact, H-bonding has already been suggested as a key factor in the molecular assembly of amino acid-based surfactants on monolayers and micelles.[30,36] For example, Stine replaced the hydrogen on the amide nitrogen with a methyl group that removed the H-bonding capacity of *N*-stearoylvaline.[37] After preparing monolayer films, he observed a change from anisotropic dendritic domains to isotropic round domains resembling those of fatty acids.[38] Hühnerfuss and co-workers also implied the importance of H-bonding in chiral discrimination studies of *N*-stearoylalanine monolayers by pressure-area isotherm and infrared reflection-absorption spectroscopy studies.[39] Furthermore, Huang and coworkers showed that achiral amphiphilic barbituric acid (BA) derivatives can form spiral domains in Langmuir-Blodgett (LB) films.[40] In this case, it was suggested that the directional H-bonding in BA molecules determined the morphology of the supramolecular aggregations. The above results lead to the hypothesis in the present experiments with *N*-stearoylglutamic acid that the carboxylic acid group attached to the chiral center imposes a geometric restriction on the formation of an H-bonding network. Experiments done as a function of pH, divalent ion content, temperature, as well as molecular modeling help to reinforce this idea.

$_{L}$-enantiomeric and racemic *N*-SGA were synthesized from stearol chloride and glutamic acid as reported earlier.[41] The melting points and heats of fusion of the

compounds were measured with a Perkin-Elmer Pyris 1 Differential Scanning Calorimeter (DSC). Samples of 7-8 mg were weighted on an analytical balance and sealed in aluminum pans. Heating thermograms were acquired in the range from 25 to 150 ^{o}C at a scan rate of 10 ^{o}C/min. The heat of fusion was calculated directly on the Perkin-Elmer software.

Powder x-ray diffraction (XRD) was carried out with a Bruker D8 Diffractometer in Bragg-Brontano mode with Cu K_{α} radiation at room temperature. Powder samples of $_{L}$-enantiomeric and racemic *N*-SGA compounds were spread on the sample holder and pressed with a glass slide. The data were corrected at angles from 1.500^{o} to 60.060^{o}.

Domain images were acquired in procedures described in Chapter II. Image-Pro Plus version 4.0 (Media Cybernetics) was employed to obtain statistics of the domain sizes for the racemic monolayers. Space filling molecular models were generated with ACD/ChemSketch and 3D Viewer (Advanced Chemistry Development Inc., Canada).

Results and Discussion

Domain Morphology

Langmuir films of enantiomeric and racemic *N*-SGA were formed on an acidified subphase at pH = 2.1 with 10 mM NaCl. The surfactant was spread at the interface from solutions containing 0.05 mol% TR-DHPE for visualizing domain formation by epifluorescence microscopy. The monolayers were compressed to 20 mN/m at 21.5 ^{o}C and anisotropic feather-like domains were observed in the enantiomeric monolayers as shown in Figure 14a. The typical size of the spine was 40-60 μm in length and 4.5-7.5

μm in width. Vertebrae branched out of the spine with sizes varying from 5.5 to 12 μm. Curiously, they branched out only on one side of the spine and only in one direction with respect to the long axis of the domain. Such phase domains could be observed at pressures as low as 10 mN/m. When the monolayer was further compressed to 30 mN/m, the microstructure morphology of the domains did not change significantly, although some of the spines were broken as signified in Figure 14b.

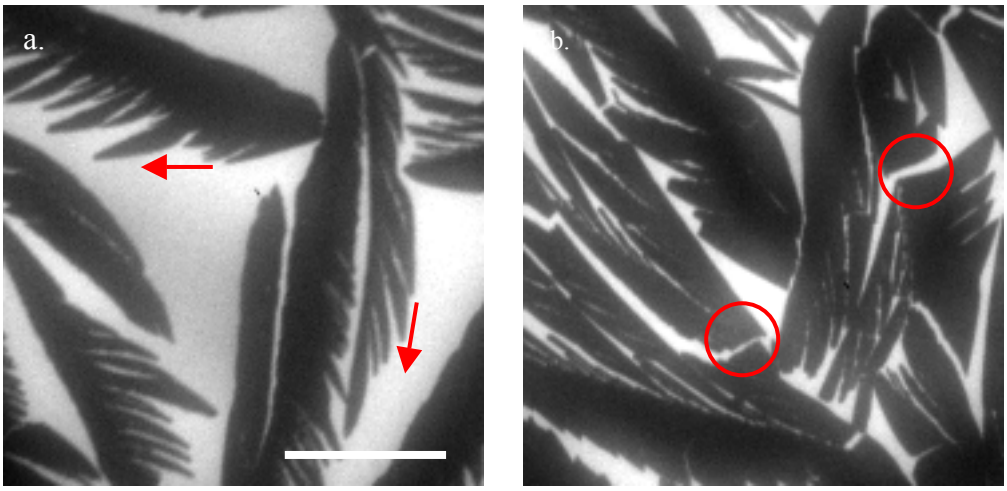

Figure 14. Domains of an *N*-SGA $_{L}$-enantiomeric monolayer on a pH = 2.1, 10 mM NaCl subphase. The scale bar represents 20 microns. The surface pressures are (a) 20 mN/m, (b) 30 mN/m, respectively.

The domain size in racemic *N*-SGA monolayers was found to be much smaller than for the pure enantiomer and no domains could be found at surface pressures below 28 mN/m. They readily formed, however, above this pressure (Figure 15a). Statistical

analysis of these isotropic domains at 30 mN/m was performed on 146 spots. The average size was 4.1 μm with the overwhelming majority of the domains falling within a size range of 3.5 to 5.5 μm (Figure 15b). The lack of asymmetry in the domain morphology almost certainly indicates a lack of chiral segregation between the $_D$ and $_L$ enantiomers. Instead, the isotropic nature of the domains suggests the $_D$ and $_L$ molecules pack together, which cancels out any asymmetry in the line tension.

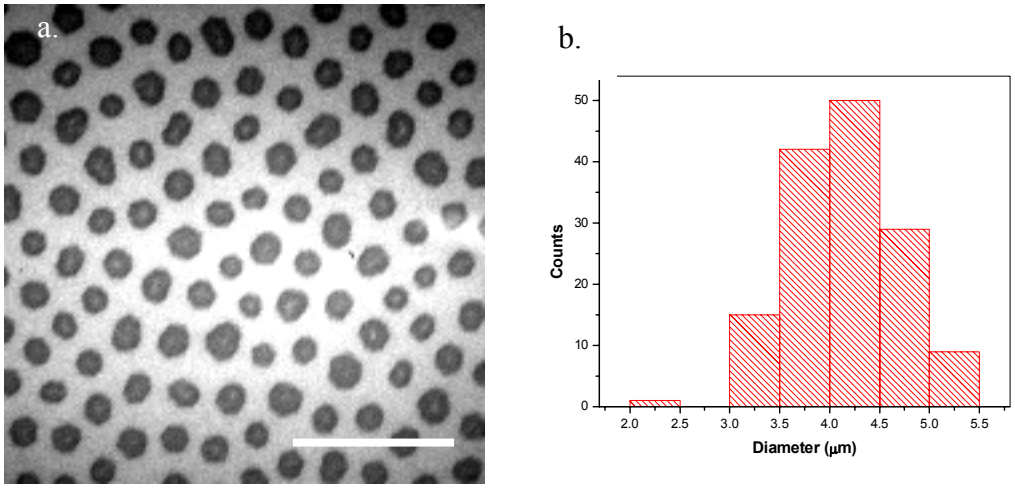

Figure 15. (a). Domains of an *N*-SGA racemic monolayer on a pH = 2.1, 10 mM NaCl subphase. The scale bar represents 20 microns, images were taken at 30 mN/m. (b). A histogram of domain sizes over the 146 samples.

Melting Temperatures

The thermal phase transition results measured by DSC in bulk *N*-SGA are tabulated in Table I. The racemic surfactants display higher melting points and fusion

enthalpies than the enantiomers. The 23.5 kcal/mol difference in the enthalpies of fusion indicates stronger molecular interaction in the racemic crystals. The increase in entropy upon fusion is about 55.9 cal/K mol greater in the case of the racemic crystals. This suggests that they are better ordered in the crystalline solid phase than the enantiomeric crystals. In contrast to the bulk, epifluorescence microscopy studies demonstrated that the two-dimensional domains of the racemic monolayers actually melted at a lower temperature than the $_{L}$-enantiomeric domains (27 ^{o}C vs. 31 ^{o}C at 30 mN/m).

Table I. Melting points, fusion enthalpies and entropies of *N*-Stearoylglutamic acid molecules

Samples	Melting Point, T_f	Enthalpy, ΔH_f^o	Entropy, ΔS_f^o
	K	kcal/mol	cal/K/mol
$_{L}$-Enantiomer	387.4	24.7 ± 1.5	64.0 ± 4.0
Racemic Compound	401.9	48.2 ± 1.7	119.9 ± 4.2

$\Delta S_f^o = \Delta H_f^o / T_f$

X-ray Diffraction Patterns

The bulk *N*-SGA racemic compound has a higher degree of crystallinity than the enantiomer as demonstrated by their powder x-ray diffraction patterns as shown in Figure 16. Diffraction peaks were found at d-spacings of 42.41, 21.20, 14.28, 10.60, 8.48 and 7.06 angstrom in both samples, while the racemate has sharper peaks. This indicates that molecules in the racemate sample are better ordered in bulk. Unfortunately, we were unable to grow crystals of high enough quality to solve their crystal structures. The samples seem to have order only along one direction. The first six peaks can be indexed to be (001), (002), (003), (004), (005) and (006). Although it is hard to index peaks at the angle ranges from 20^{o} to 25^{o}, it did not escape our notice that the racemate compound has more distinct diffraction peaks in the range. The samples were also checked with small angle x-ray scattering (SAXS) from angle 0.005^{o} to 4.500^{o}. There is no other peak with d-spacings larger than 42.41Å. The distance is approximately twice that of the monolayer thickness as measured with atomic force microscopy on LB films of the same compounds.[42]

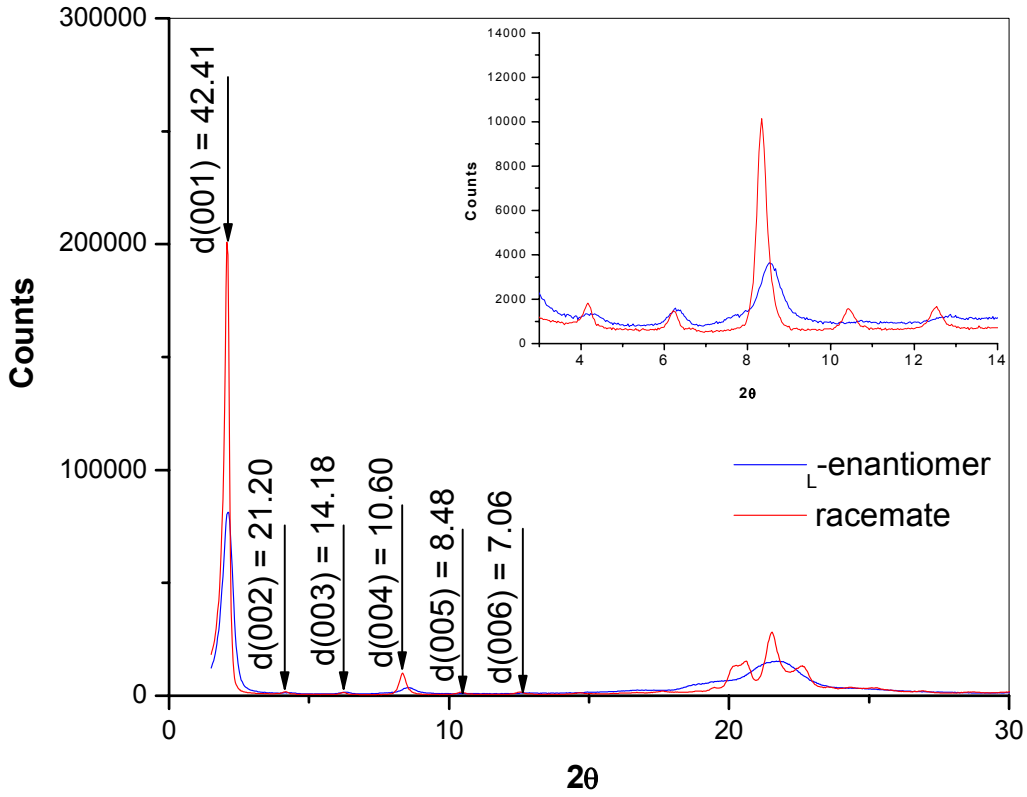

Figure 16. Powder x-ray diffraction patterns of $_{L}$-enantiomeric and racemic *N*-SGA compounds.

Molecular Models

In the case of the thin film, the morphology and thermal stability of the domains is probably largely mediated by the directionality of the H-bonding. Space-filling molecular models are shown in Figure 17. The α-carboxyl group attached to the chiral center is seen to have a significant effect on the molecular packing. Furthermore, shorter H-bond lengths are possible in the model for the enantiomeric monolayers. This is significant as shorter bond lengths allow stronger hydrogen bonding and increase

thermal stability. Indeed, this is exactly what is found in the case of proteins, amide-amide hydrogen bonding energies vary widely in proteins. The N-H---O=C hydrogen bond geometries of biomacromolecules can vary in length from 1.96-2.26 Å and bond angles can vary from 152-161°.[43] This leads to bond energy variations between 2-10 kcal/mol. Thus, it is already well established that H-bond strength in amide-aminde bonds is very sensitive to the distance and angle between the NH and O=C groups.

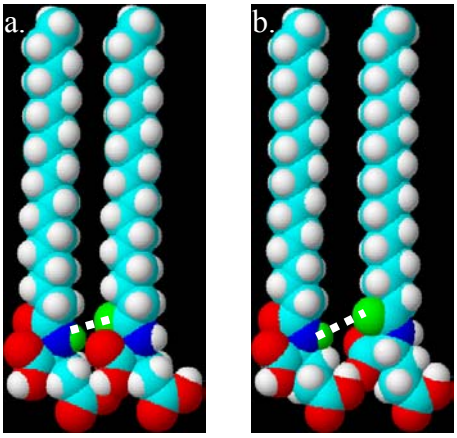

Figure 17. Space filling models of (a) $_{L:L}$ and (b) $_{D:L}$ *N*-SGA molecular interactions. The Carbon, Nitrogen, Oxygen and Hydrogen atoms are in cyan, blue, red and white, respectively. Atoms involved in H-bonding atoms are colored in green.

The above findings for *N*-SGA show some analogy to thermal transition and monolayer stability studies of stearoylserine methyl ester (SSME).[30] In that case it was also found that the racemic crystals melt at a higher temperature than those of the enantiomers. Unfortunately, melting temperatures are not available for monolayer domains in that case. However, pressure-area isotherm data as a function of temperature

suggest that more tightly packed portions of enantiomeric monolayers are thermally more stable. This is tantalizing evidence that a reversing of the melting point order of enantiomers and racemates when going from three dimensions to two dimensions might be general. Such a hypothesis will need to be tested on a wide range of systems to verify its validity.

Monolayer Stability with pH and Divalent Cations

Under the conditions described above (pH 2.1), the carboxylic acid groups of *N*-SGA should be fully protonated. Indeed, confining a two-dimensional array of such groups to a thin film interface actually increases their pK_a relative to the bulk.[44] In order to induce some deprotonation, the pH of the subphase was increased to 6.2 at 30 mN/m. In this case, repulsive electrostatic forces are directly introduced into the system and the α-carboxylic acid group of the glutamic acid should be ionized to a greater extent than the γ-carboxylic acid due to its closer proximity to the amide bond.[45] Figures 18a&b show the epifluorescence micrographs of the $_L$-enantiomeric and the racematic monolayers, respectively. As can be seen, the increase in pH profoundly affects the former system while leaving the latter almost intact. In fact, the domains from the chiral system have almost completely disappeared with only a few very small spots found. By contrast, the average domain diameter of the racemate was reduced modestly from 4.1 to 3.2 μm. This data shows the profound effect that electrostatic forces can have on very closely packed structures such as chiral domains. On the other hand, the more loosely packed racemic domains are far less affected.

In a final set of experiments, we wished to discern the effects of divalent metal ions on enantiomeric and racemic Langmuir monolayers. This was proposed because it is believed that the electrostatic bridging of the carboxylic acids should be much stronger than the effect of hydrogen bonding. Indeed, it is well established that the complexation of metal ions with the headgroups of fatty acids generally causes the Π-A isotherm of the monolayer to be more condensed.[46] This in turn affects the alkyl chain conformation as noted by ellipsometry and grazing incidence X-ray diffraction (GID) techniques.[47,48] In the present studies, the $_{L}$-enantiomeric and racemic monolayers were investigated upon the addition of Cu^{2+} at pH 6.2. Here, we observed that even the domain formation in the racemic monolayers was completely disrupted as shown in Figure 18c&d. Cu^{2+} ions are specifically known to have strong chelating effects with surface-confined carboxylic groups.[49,50] Most likely, such strong interactions overrode weaker intermolecular amide-amide H-bonding.

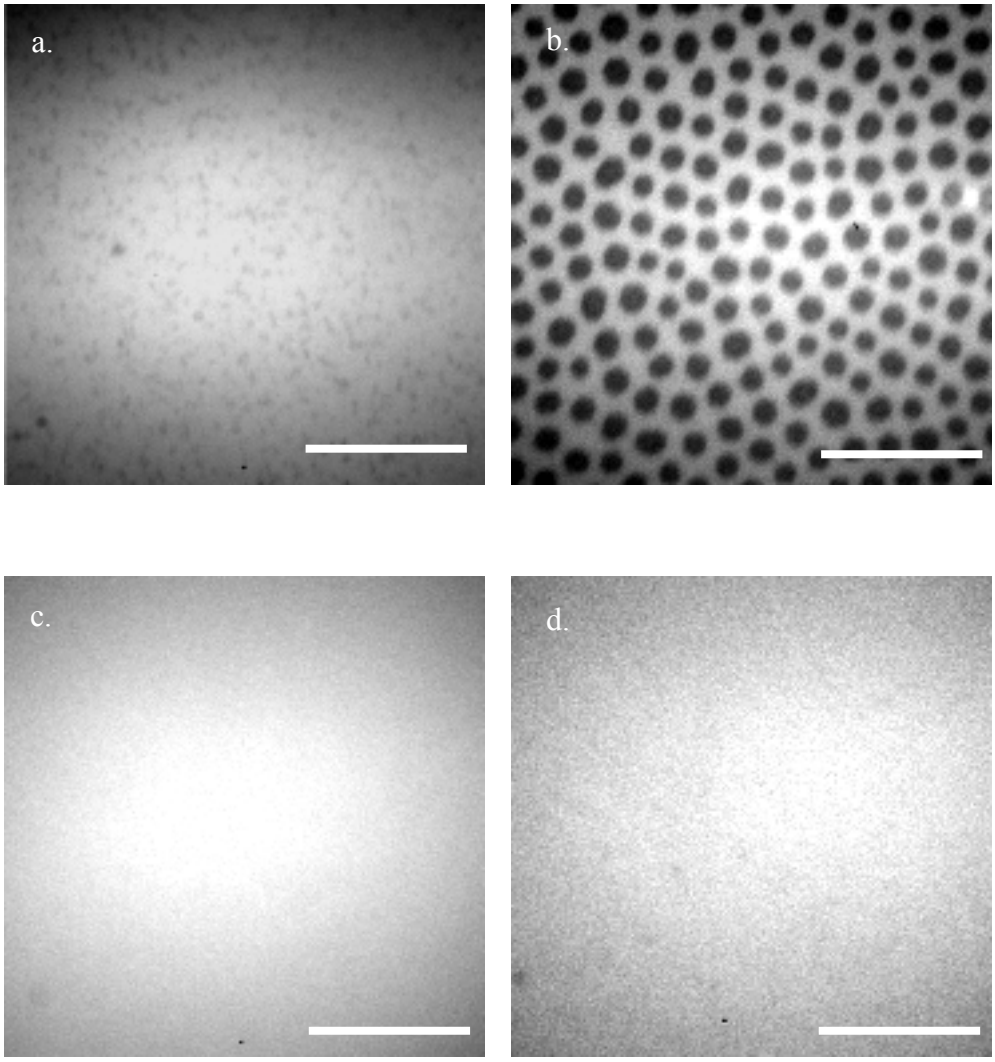

Figure 18. Domains of $_{L}$-enantiomeric (a,c) and racemic monolayers (b,d) were observed on NaCl and $CuCl_2$ subphase respectively. The bars represents 20 microns.

Conclusions

Herein we have demonstrated that the pure enantiomeric form of the amino acid based surfactant, *N*-stearoylglutamic acid, forms asymmetric phase domains in two dimensions at the air/water interface. These domains are more thermally stable than those found from the corresponding racemate. This result is exactly the opposite of bulk behavior where the racemate is more stable. Studies as a function of pH, molecular modeling data, as well as literature president point to more favorable hydrogen bonding in two dimensions to explain this inversion.

CHAPTER IV

INVESTIGATIONS OF HYDROGEN BONDING IN AMINO ACID AMPHIPHILES AT AIR/WATER INTERFACE BY VIBRATIONAL SUM FREQUENCY SPECTROSCOPY (VSFS)

Introduction

Hydrogen bonding (H-bonding) is an essential component of structure and function of biological molecules.[43] There is a great deal of literature concerning the effect of H-bonds formation on three-dimensional structures of polypeptides and proteins. The α-helix and β-sheet structures are two good examples of how the secondary structures of proteins are influenced by amide-amide H-bonds.[51] However, there are very few reports about hydrogen bonding on protein interfacial structure. It is still a very challenging experimental problem to probe the surface structures of proteins although their interfacial properties are recognized to be important in fields such as medical implantation, drug discovery and biological sensor development.[52-54]

This problem can now be tackled with a new and powerful surface technique called sum-frequency generation (SFG), which is able to selectively probe molecules at the interfaces of liquid.[55] Protein adsorption on various surfaces has been studied by VSFS during the past four years.[25,56,57] Information on the molecular response of the protein and water molecule alignment under proteins at different interfaces has been obtained. However, the surface structures of proteins, such as hydrogen bonding, still cannot be resolved at the molecular level because of the complexity of protein structures.

N-acyl amino acids are one category of lipoamino acids, which have structural similarity to protein surface structures. Their molecular structures are shown in Figure 1. They are analogs to *C*-terminal peptides, which have a peptide bond and an amino acid residue in the end. The molecules are thus useful mimic systems to investigate protein interfacial structure. In particular, *N*-SG molecules mimic aspartic acid residues on the hydrophilic surface of proteins, which plays an important role in ion channel formation.[58] The investigation of interfacial properties of *N*-SG monolayers formed at air/water interface should provide some insights into aspartic acid rich domains in proteins. The NH stretch signal from an amide group is resolved for the first time with the VSFS technique. The vibrational mode can be used as fingerprint of amide-amide H-bond formation for structural analysis and molecular recognition.[59] H-bond formation between carboxylic acid groups was also investigated on the *N*-acyl amino acids assembly at air/water interface.

The VSFS experiments were carried out under the conditions as discussed in Chapter II. Briefly, $_{L}$-*N*-SGA, $_{L}$-*N*-SA and *N*-SG monolayers were formed on a Nima Langmuir trough. If not specified, $_{L}$-enantiomers were used in this chapter. A Phosphate Buffer Saline (PBS) solution was prepared as the subphase for the spreading of the molecules. Spectra were taken with the ssp polarization combination mode. The acquired spectra were processed and plotted in Origin 7.0 (OriginLab Corp.). Molecular models are drawn in ACD-ChemSketch.

Results and Discussion

Hydrogen Bonding in N-SA Monolayers

Shown in Figure 19 is the spectrum collected from $_{L}$-*N*-SA monolayers on a pH = 2.5 subphase. Four bands are resolved from 2700 to 3000 cm^{-1}, corresponding to the CH moieties' vibrational modes. The band at 2874 cm^{-1} is the symmetric stretch of the CH_3 group. In these molecules, this band should correspond to the methyl groups at the end of the hydrocarbon chains. The peak at 2834 cm^{-1} was assigned to the methylene groups of the chains. The band is not detectable in VSFS if the chain is in the all-trans configuration. Therefore, gauche defects are present in the monolayer.[60] The peak at 2936 cm^{-1} corresponds to the asymmetric stretch of the CH_3 group. Two peaks were found in the range from 3000 to 3550 cm^{-1} as shown in Figure 19b. A peak at 3311 cm^{-1} was clearly resolved. This peak was assigned to the hydrogen bonded NH stretch in the amide group.[61] The peak at 3050 cm^{-1} was previously reported in the VSFS study of a fatty acid at the air/water interface. It was assigned to disrupted H-bonds at the interfaces because the authors argued that formation of cyclic dimers was very unlikely for fatty acid monoalyer.[62] With this same molecule, the study of IRRAS suggested there are two forms of carboxylic acid dimers at the air/water interface at different surface pressures.[61] It was clearly shown that a peak at 1730 cm^{-1} changed to 1705 cm^{-1} with increasing surface pressure, indicating out-of-plane cyclic dimer formation on $_{L}$-*N*-SA at a surface pressure of 20 mN/m. Data was also collected at 30 mN/m on $_{L}$-*N*-SA monolayers as shown in Figure 20. Based on this investigation and other literature, a molecule model of the H-bond formation in $_{L}$-*N*-SA at an interface was proposed in Figure 21a.

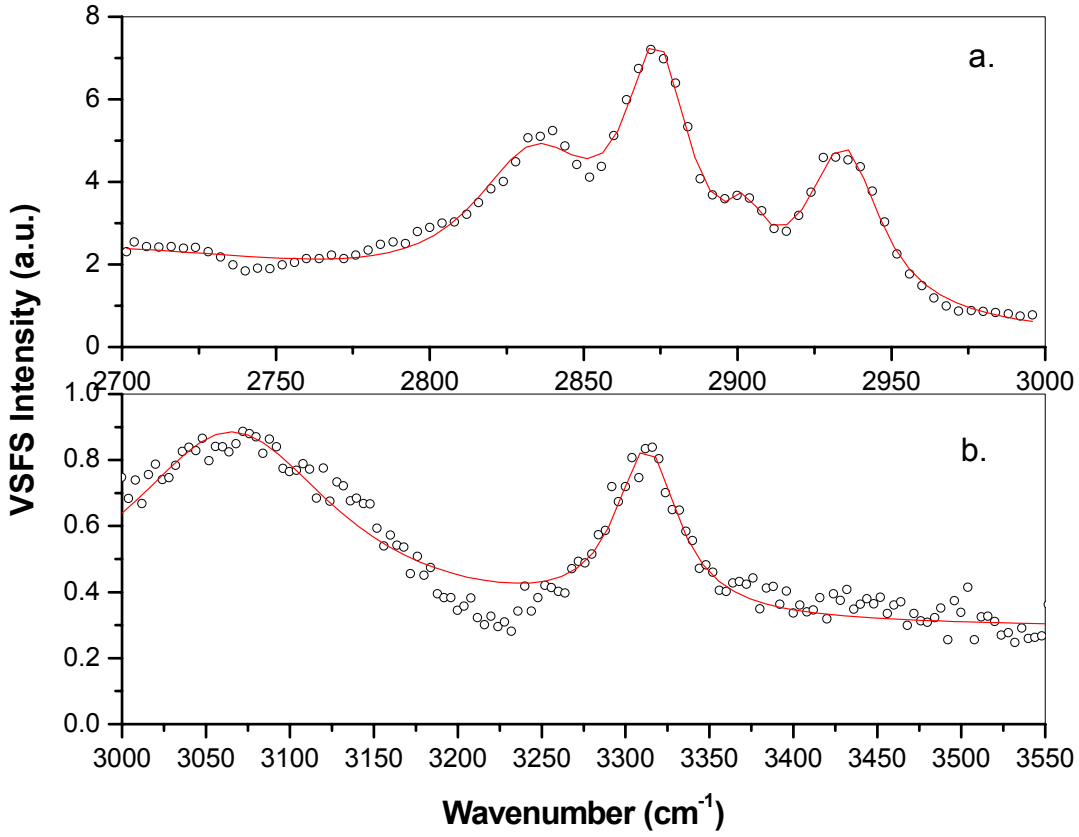

Figure 19. VSFS spectrum of *N*-stearoyl-$_L$-alanine acquired at pH = 2.5 (PBS), $\Pi = 20$ mN/m. a. the CH region, four bands at 2834, 2874, 2902 and 2936 cm^{-1} were resolved; b. the OH and NH region, two bands at 3060 and 3311 cm^{-1} were resolved.

Hydrogen Bonding in Other N-acyl Amino Acid Monolayers

The H-bond formation of other amino acid amphiphiles was also investigated. VSFS spectra of $_L$-*N*-SA, $_L$-*N*-SGA and *N*-SG are shown together in Figure 20. The NH

peak in $_{L}$-*N*-SGA was found to be 3341 cm^{-1}, which is 30 cm^{-1} higher than that of *N*-SA. It clearly indicates that the H-bond strength is smaller than that of $_{L}$-*N*-SA. This is presumably due to the larger size of glutamic acid residues. Furthermore, a peak at 3560 cm^{-1} shows up distinctly. This peak is assigned to a monomeric form of the carboxylic acid.[63] Again, because of steric hindrance in $_{L}$-*N*-SGA, the carboxylate group may not able to form a cyclic dimer as it does in $_{L}$-*N*-SA. The molecular model is shown in Figure 21b. The NH stretching peak of *N*-SG is very weak as shown in Figure 20c. There is a strong reason to argue that H-bond formation is present in this monolayer as the *N*-SG molecules readily form highly ordered monolayers even at very low surface pressure. This stability comes from the hydrogen-bonding network. Indeed, only CH_3 vibration modes are found from its VSFS spectrum. This indicates that the molecules contain few defects. Because the VSFS was operated at ssp mode, dipoles parallel to the surface would not show up strongly in the spectrum. A molecular model of this system is shown in Figure 21c.

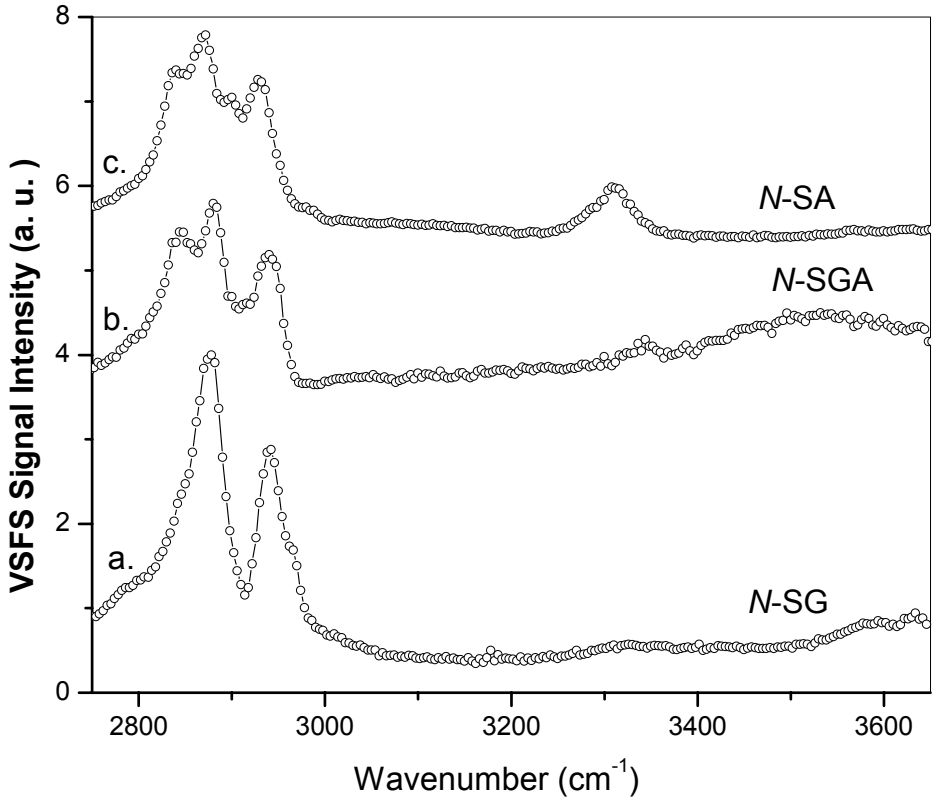

Figure 20. VSFS spectra of *N*-stearoylalanine (*N*-SA), *N*-stearoylglutamic acid (*N*-SGA) and *N*-stearoylglycine (*N*-SG) on a pH = 2.5 PBS surphase at $\Pi = 25$ mN/m.

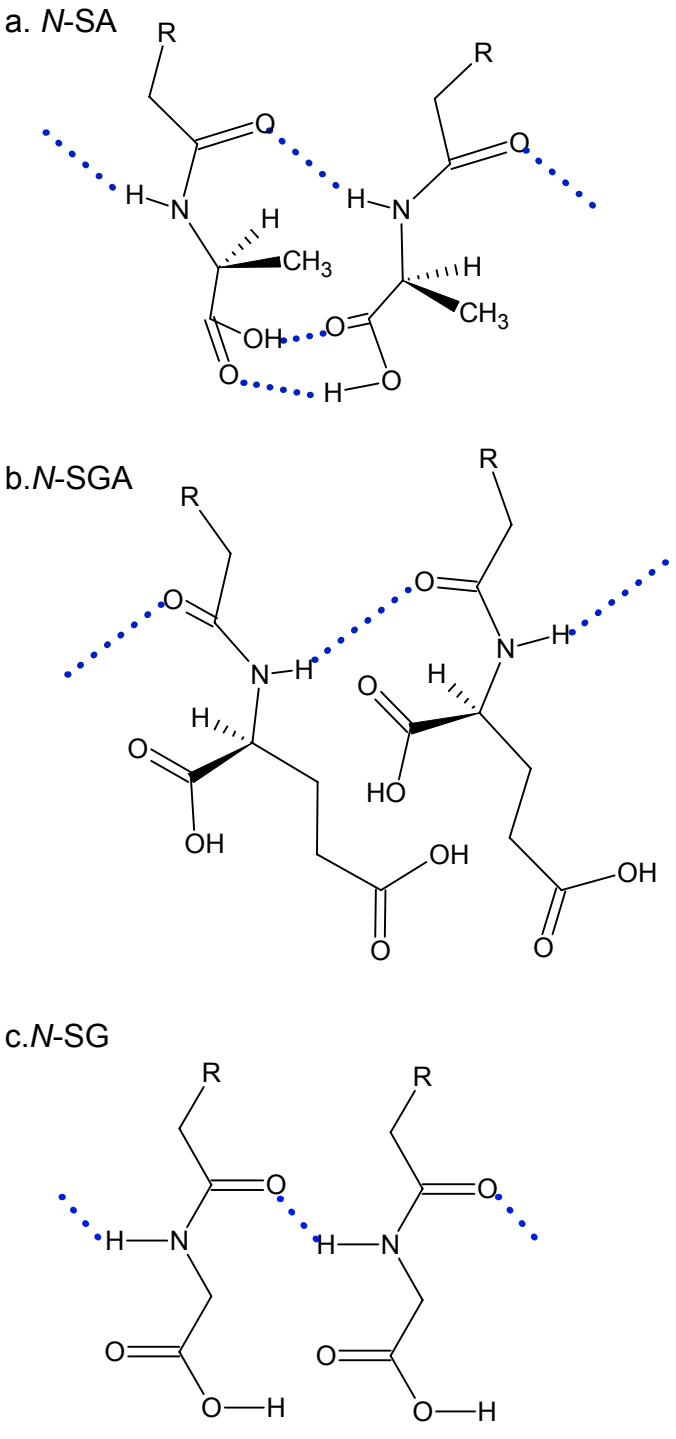

Figure 21. Schematic illustration of the formation of intermolecular hydrogen bonds between amide groups and carboxylic acid groups. R is the hydrocarbon chain -$C_{16}H_{34}$.

In a final set of experiments, hydrogen bond formation between *N*-SG molecules was investigated at different surface pressures. Figure 22 shows the VSFS spectra of the monolayer formed on a pH = 2.5 PBS subphase. At surface pressures as high as 50 mN/m, there is a distinct peak at 3050 cm^{-1}. This indicates that the carboxylic groups started to form dimers at this pressure. Hydrogen bonding between carbonyl and hydroxyl groups formed only when the molecules were sufficiently close.

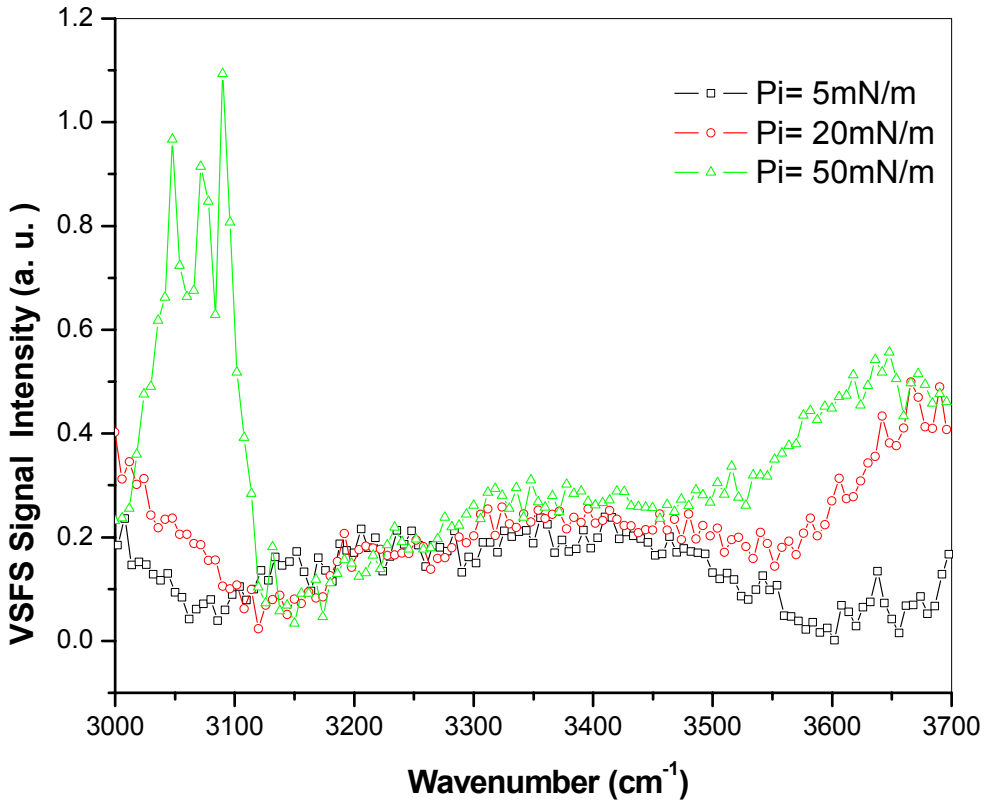

Figure 22. VSFS spectra of *N*-SG at different surface pressures. The peak at 3050 cm^{-1} shows up at high surface pressure.

Summary

Hydrogen bond formation in *N*-acyl amino acids at the air/water interface was investigated. The NH stretch frequency can be correlated with the size of the amino acid residues on the molecules. It was found that smaller amino acid residues such as alanine gave rise to a peak at lower frequency. This indicates that the strength of H-bonds among amide groups is stronger due to the smaller size of the amino acid residues. The hydrogen bonding between carboxylic groups is also found to be sensitive to the distance between the two groups.

CHAPTER V

SUMMARY

During the course of my study in the chemistry department at Texas A&M University, my major interest focused on biological surface chemistry. This is a dynamic and interdisciplinary field that is both challenging and rewarding for graduate study. The problems in this area are experimentally challenging because there are not many tools that have specific access to the surface of biomolecules. In other words, it is difficult to differentiate surface signals from bulk ones. Another challenge is the difficulty of data interpretation. The complexity of the structure and dynamics of biomolecules is one thing. The difficulty of interpreting results obtained from aqueous environments is another. It is notoriously difficult to characterize surface properties at a liquid interface. For example, the alignment of water molecules at interfaces is still a subject for speculation.

The approach taken in this thesis is to find simple model systems and address the complicated surface problems in real biological environments. Amino acid-based surfactants (AAS) were investigated because I believe that they can provide valuable information about protein interfacial properties, given their surface activity and biological relevance. Indeed, the molecules shown in Figure 1 have the same chirality that is prevalent in biological molecules. They also have peptide bonds that are essential for intermolecular hydrogen bonding. They possess amino acid residues that mimic hydrophilic portion of protein surfaces. More importantly, these molecules are amphiphilic, and they are able to form monomolecular films at the air/water interface,

which is very convenient for manipulations and thus provides an opportunity to study the dependence of molecular packing and phase behavior on molecular interactions.

The first part of my research dealt with chiral molecular interaction. The choice of AAS was motivated by the attractiveness of their structures. All the naturally occurring amino acids (except glycine) have a chiral center. After being conjugated to a hydrophobic hydrocarbon chain, they assemble at the air/water interface to form Langmuir monolayers. The microstructures of the monolayers were investigated by epifluorescence microscopy, which took advantage of the variable partitioning of the fluorescence dyes in the two-dimensional phases. From the domain morphology study, a correlation between molecular chirality and domain handedness was established. Further observations of melting behavior of the phase domains at a two-dimensional interface revealed the striking fact that the chiral molecular interaction strength in the enantiomeric and racemic forms can be totally inverted compared to that of three-dimensional crystals. There are a wide variety of amino acids derivatives that can be used for this type of study. This system is thus valuable to probe chiral molecular interaction.

In the second set of experiments, the focus switched from chiral molecular interactions to the interfacial properties of these molecules at the air/water interface. In particular, hydrogen bonding network formation was investigated. From the comparison of three *N*-stearoyl amino acids, it was established that the strength and the direction of the amide-amide hydrogen bonding at interfaces are affected by the size of the amino acid residues. This came from the discovery of the NH stretching mode in the VSFS

spectra. It was the first time that the peak was resolved from molecules at an interface with this technique. The frequency of the peak gives some information about the strength of the hydrogen bonding among amide groups. It is expected that among the glutamic acid derivatives, the hydrogen bonds are weaker due to their larger residue size. Indeed, the frequency of NH peak of alanine derivatives is 30 cm^{-1} lower. The glycine derivative is expected to give the strongest hydrogen bonding, and thus the lowest NH peak frequency. However, the peak was not found our VSFS spectra with ssp. This leads to the modified model about the orientation of the head groups. It is speculated that the NH in *N*-SG is parallel to the surface and thus not active in the ssp mode. On the contrary, due to the asymmetric properties of *N*-SA and *N*-SGA molecules, the molecules are titled at the air/water interface and thus become active with this polarization combination. Together with recent studies of *N*-SA monolayers by IRRAS, a molecular model of hydrogen bonding between carboxylic groups is proposed. Now, there is a more detailed understanding of the hydrogen bonding among amino acids residues which may be similar to the hydrophilic surfaces of proteins. The property and the function of proteins may have something to do with the hydrogen bonding at interface.

Another interesting note to this thesis is about surfactant behavior on biomembrane surfaces. This problem has been extensively studied and reported previously. Surfactants are commonly applied to solublize membrane proteins from the cell membranes. Experiment results and literature research show that conventional surfactants such as SDS completely solubilize bilayers at concentrations close to their

CMC. Although it was also reported that SDS can extract Ca^{2+}-ATPase from liposomes before solulilizing them, there is very little selectivity of the surfactants towards the membrane components. By contrast, amino acid-based surfactants were found to be able to selectively remove hydrophobic components from the biomembranes without solubilizing them. It is speculated that hydrogen bonding plays an important role in the surfactants aggregation as well. They are most likely aggregated through hydrogen bonding, and it thus becomes difficult for the molecules to partition into membranes like other surfactants, such as SDS, Trixton X-100 and CTAB. Instead of forming mixed micelles with lipid, they can more favorably remove hydrophobic dyes from the lipid bilayers. From the experiments conducted on supported lipid bilayer doped with fluorescence dyes, it was found that *N*-SG could selectively remove the more hydrophobic Texas-Red DHPE but not the NBD-DHPE. This finding may lead to the development of agents that can selectively remove ligands such as anthrax toxin from membrane surfaces. Because of their biocompatibility, the amino acid-based surfactants may have great potential for biomedical applications.

REFERENCES

(1) Kimura, A. *Prog.Ind.Microbiol.* **1986**, *24*, 329-334.

(2) Yagi, H.; Corzo, G.; Nakahara, T. *Biochim.Biophys.Acta* **1997**, *1336*, 28-32.

(3) Peypoux, F.; Laprevote, O.; Pagadoy, M.; Wallach, J. *Amino Acids* **2004**, *26*, 209-214.

(4) Nnanna, N. A.; Xia, J. *Protein-Based Surfactants*; Marcel Dekker: New York, 2001.

(5) Huang, S. M.; Bisogno, T.; Petros, T. J.; Chang, S. Y.; Zavitsanos, P. A., et al. *J.Biol.Chem.* **2001**, *276*, 42639-42644.

(6) Langmuir, I. *J.Am.Chem.Soc.;* **1917**, *39*, 1848-1906.

(7) Gaines, G. L. Jr. *Insoluble Monolayers at Liquid-gas Interfaces*; Interscience Publishers : New York, 1966.

(8) Petty, M. C. *Langmuir-Blodgett Films*; University Press: Cambridge, UK, 1996.

(9) Adamson, A. W.; Gast, A. P. *Physical Chemistry of Surfaces*; John Wiley & Sons: New York, 1997.

(10) McConnell, H. M. *Annu.Rev.Phys.Chem.* **1991**, *42*, 171-195.

(11) McConnell, H. M.; Moy, V. T. *J.Phys.Chem.* **1988**, *92*, 4520-4525.

(12) Nandi, N.; Vollhardt, D. *Chem.Rev.* **2003**, *103*, 4033-4075.

(13) Parazak, D. P.; Uang, J. Y. J.; Turner, B.; Stine, K. J. *Langmuir* **1994**, *10*, 3787-3793.

(14) Jacques, J.; Collet, A.; Wilen, S. H. *Enantiomers, Racemates, and Resolutions*; Wiley: New York, 1981.

(15) Helenius, A.; Simons, K. *Biochimica et Biophysica Acta* **1975**, *415*, 29-79.

(16) Kragh-Hansen, U.; le Maire, M.; Moller, J. V. *Biophys.J* . **1998**, *75*, 2932-2946.

(17) Jungermann, E.; Gerecht, J. F.; Krems, I. J. *J.Am.Chem.Soc.* **1955**, *78*, 172-174.

(18) Sivasamy, A.; Krishnaveni, M.; Rao, P. G. *J.Am.Oil Chem.Soc.* **2001**, *78*, 897-902.

(19) Ohta, A.; Ozawa, N.; Nakashima, S.; Asakawa, T.; Miyagishi, S.

Colloid.Polym.Sci. **2003**, *281*, 363-369.

(20) Takehara, M.; Takizawa, K.; Yoshimuri.I; Yoshida, R. *J.Am.Oil Chem.Soc.* **1972**, *49*, 157.

(21) Zhang, Y. J.; Song, Y. L.; Zhao, Y. Y.; Li, T. J.; Jiang, L., et al. *Langmuir* **2001**, *17*, 1317-1320.

(22) Shen, Y. R. *Appl.Phys.B* **1999**, *68*, 295-300.

(23) Wei, X.; Hong, S. C.; Lvovsky, A. I.; Held, H.; Shen, Y. R. *J.Phys.Chem.B* **2000**, *104*, 3349-3354.

(24) Kim, G.; Gurau, M. C.; Lim, S. M.; Cremer, P. S. *J.Phys.Chem.B* **2003**, *107*, 1403-1409.

(25) Kim, G.; Gurau, M.; Kim, J.; Cremer, P. S. *Langmuir* **2002**, *18*, 2807-2811.

(26) Axelrod, D.; Koppel, D. E.; Schlessinger, J.; Elson, E.; Webb, W. W. *Biophys.J* . **1976**, *16*, 1055-1069.

(27) Tamm, L. K.; McConnell, H. M. *Biophysical Journal* **1985**, *47*, 105-113.

(28) Yuan, Y. H.; Velev, O. D.; Lenhoff, A. M. *Langmuir* **2003**, *19*, 3705-3711.

(29) Arnett, E. M.; Harvey, N. G.; Rose, P. L. *Acc.Chem.Res.* **1989**, *22*, 131-138.

(30) Harvey, N. G.; Mirajovsky, D.; Rose, P. L.; Verbiar, R.; Arnett, E. M. *J.Am.Chem.Soc.* **1989**, *111*, 1115-1122.

(31) Zepik, H.; Shavit, E.; Tang, M.; Jensen, T. R.; Kjaer, K., et al. *Science* **2002**, *295*, 1266-1269.

(32) Heath, J. G.; Arnett, E. M. *J.Am.Chem.Soc.* **1992**, *114*, 4500-4514.

(33) Stine, K. J.; Uang, J. Y. J.; Dingman, S. D. *Langmuir* **1993**, *9*, 2112-2118.

(34) Gericke, A.; Huhnerfuss, H. *Langmuir* **1994**, *10*, 3782-3786.

(35) Nandi, N.; Vollhardt, D. *Colloids Surf., A* **2001**, *183*, 67-83.

(36) Shinitzky, M.; Haimovitz, R. *J.Am.Chem.Soc.* **1993**, *115*, 12545-12549.

(37) Stine, K. J.; Leventhal, A. R.; Parazak, D. P.; Uang, J. Y. J. *Enantiomer* **1996**, *1*, 41-48.

(38) Honig, D.; Mobius, D. *Thin Solid Films* **1992**, *210*, 64-68.

(39) Hühnerfuss, H.; Neumann, V.; Stine, K. J. *Langmuir* **1996**, *12*, 2561-2569.

(40) Huang, X.; Li, C.; Jiang, S. G.; Wang, X. S.; Zhang, B. W., et al. *J.Am.Chem.Soc.* **2004**, *126*, 1322-1323.

(41) Zhang, Y. J.; Song, Y. L.; Zhao, Y. Y.; Li, T. J.; Jiang, L., et al. *Langmuir* **2001**, *17*, 1317-1320.

(42) Zhang, Y. J.; Jin, M.; Lu, R.; Song, Y. L.; Jiang, L., et al. *J.Phys.Chem.B* **2002**, *106*, 1960-1967.

(43) Jeffrey G.A. *An Introduction to Hydrogen Bonding*; Oxford University Press: New York, 1997.

(44) Davies, J. T.; Rideal, E. K. *Interfacial Phenomena*; Academic Press: New York, 1963.

(45) Voet, D.; Voet, J. G. *Biochemistry*; John Wiley & Sons: New York, 1995.

(46) Gaines, G. L. Jr. *Insoluble Monolayers at Liquid-gas Interfaces*; Interscience Publishers : New York, 1966.

(47) Bettarini, S.; Bonosi, F.; Gabrielli, G.; Martini, G.; Puggelli, M. *Thin Solid Films* **1992**, *210*, 42-45.

(48) Shih, M. C.; Bohanon, T. M.; Mikrut, J. M. *J.Chem.Phys.* **1992**, *96*, 1556-1559.

(49) Major, R. C.; Zhu, X. Y. *J.Am.Chem.Soc.* **2003**, *125*, 8454-8455.

(50) Dynarowicz-Latka, P.; Dhanabalan, A.; Oliveira, O. N. *Adv.Colloid Interface Sci.* **2001**, *91*, 221-293.

(51) Rose, G. D.; Gierasch, L. M.; Smith, J. A. *Adv.Protein Chem.* **1985**, *37*, 1-109.

(52) Kenausis, G. L.; Voros, J.; Elbert, D. L.; Huang, N. P.; Hofer, R., et al. *J.Phys.Chem.B* **2000**, *104*, 3298-3309.

(53) *Proteins at Interfaces II: Fundamentals and Applications*; Horbett, T.A.,Brash, J.L., Eds; ACS Symposium Series 602; American Chemical Society: Washington, DC, 1995; Chapter 5.

(54) Seigel, R. R.; Harder, P.; Dahint, R.; Grunze, M.; Josse, F., et al. *Anal.Chem.* **1997**, *69*, 3321-3328.

(55) Eisenthal, K. B. *Chem.Rev.* **1996**, *96*, 1343-1360.

(56) Wang, J.; Buck, S. M.; Even, M. A.; Chen, Z. *J.Am.Chem.Soc.* **2002**, *124*, 13302-13305.

(57) Kim, J.; Somorjai, G. A. *J.Am.Chem.Soc.* **2003**, *125*, 3150-3158.

(58) Chen, X. H.; Tsien, R. W. *J.Biol.Chem.* **1997**, *272*, 30002-30008.

(59) Weck, M.; Fink, R.; Ringsdorf, H. *Langmuir* **1997**, *13*, 3515-3522.

(60) Guyotsionnest, P.; Hunt, J. H.; Shen, Y. R. *Phys.Rev.Lett.* **1987**, *59*, 1597-1600.

(61) Du, X.; Liang, Y. *J.Phys.Chem.B* **2004**, *108*, 5666-5670.

(62) Miranda, P. B.; Du, Q.; Shen, Y. R. *Chem.Phys.Lett.* **1998**, *286*, 1-8.

(63) Lin-Vien, D.; Colthup, N. B.; Fateley, W. G.; Grasselli, J. G. *The Handbook of Infrared and Raman Characteristic Frequencies of Organic Molecules*; Academic Press, Inc: San Diego, 1991.

VITA

Dengliang Yang

#171 Zhangxi, Cangnan, Zhejiang Province
China, 325803

EDUCATION

M.S. in chemistry
Texas A&M University, College Station, August 2004
Advisor: Dr. Paul. S. Cremer

M.S. in advanced materials
National University of Singapore, Singapore, July 2001
Program of Singapore-MIT Alliance
Advisor: Prof. Soo Jin Chua

B.E. in biochemical engineering
Zhejiang University, Hangzhou, P. R. China, June 2000

SELECTED PUBLICATIONS

1. Yang, R.D.; Tripathy, S.; Tay, F.E.H.; Gan, L.M.; Chua, S.J. *J.Vac.Sci.Technol.,B* **2003,** *21,* 984-988.

2. Yang, R.D.; Li, Y.; Sue, H.-J. *Mat.Res.Soc.Symp.Proc.* **2003,** *775*, P9.43.1.

3. Jung, S.; Lim, S.; Albertorio, F.; Kim, F.; Curau, M.; Yang, R.D.; Holden, M.A.; Cremer, P.S. *J. Am. Chem. Soc.* **2003,** *125,*11166-11167

4. Kataoka, S.; Gurau, M.C.; Albertorio, F.; Holden, M.A.; Lim, S.; Yang, R.D.; Cremer**,** P.S. *Langmuir* **2004**,*20*, 1662-1666